GFP in living animals reveals dynamic developmental responses to ecdysone during *Drosophila* metamorphosis☆

Robert E. Ward,[1] Pamela Reid,[1] Arash Bashirullah,[1]
Pier Paolo D'Avino,[2] and Carl S. Thummel*

*Howard Hughes Medical Institute, Department of Human Genetics, University of Utah, 15 North 2030 East Rm 5100, University of Utah,
Salt Lake City, UT 84112-5331, USA*

Abstract

Studies of *Drosophila* metamorphosis have been hampered by our inability to visualize many of the remarkable changes that occur within the puparium. To circumvent this problem, we have expressed GFP in specific tissues of living prepupae and pupae and compiled images of these animals into time-lapse movies. These studies reveal, for the first time, the dynamics and coordination of morphogenetic movements that could only be inferred from earlier studies of dissected staged animals. We also identify responses that have not been described previously. These include an unexpected variation in some wild-type animals, where one of the first pairs of legs elongates in the wrong position relative to the second pair of legs and then relocates to its appropriate location. At later stages, the antennal imaginal discs migrate from a lateral position in the head to their final location at the anterior end, as leg and mouth structures are refined and the wings begin to fold. The larval salivary glands translocate toward the dorsal aspect of the animal and undergo massive cell death following head eversion, in synchrony with death of the abdominal muscles. These death responses fail to occur in rbp^5 mutants of the *Broad-Complex* (*BR-C*), and imaginal disc elongation and eversion is abolished in br^5 mutants of the *BR-C*. Leg malformations associated with the $crol^3$ mutation can be seen to arise from defects in imaginal disc morphogenesis during prepupal stages. This approach provides a new tool for characterizing the dynamic morphological changes that occur during metamorphosis in both wild-type and mutant animals.
© 2003 Elsevier Science (USA). All rights reserved.

Keywords: Ecdysone; Imaginal discs; Larval muscles; Morphogenesis; Cell death; Adult development

Introduction

Few biological events have captured the human imagination as much as insect metamorphosis. The transformation of a crawling larva into a highly mobile and sexually reproductive adult insect raises a wide range of biological questions and provides an ideal system for studying developmental timing and terminal differentiation. Not surprisingly, studies of metamorphosis have focused largely on lepidopteran insects, facilitated by their size, well-characterized hormone titers, and the ability to precisely stage their development (Gilbert et al., 1996). Over the past decade, however, our understanding of metamorphosis in the relatively small Dipteran insect, *Drosophila melanogaster,* has advanced significantly as a result of intensive molecular genetic analyses. These studies have provided insights into the molecular basis of metamorphosis, yielding initial clues regarding how hormonal effects on gene expression are transduced into such a remarkable variety of stage- and tissue-specific biological responses (Richards, 1997; Russell and Ashburner, 1996; Thummel, 1996).

In *Drosophila,* as in all holometabolous insects, metamorphosis is controlled by changes in the titer of the steroid hormone 20-hydroxyecdysone (henceforth referred to as

ecdysone). A high-titer ecdysone pulse at the end of the third larval instar triggers puparium formation, signaling the onset of metamorphosis and the prepupal stage in development (Riddiford, 1993). This is followed by another pulse of ecdysone, approximately 10–12 h after puparium formation. This prepupal ecdysone pulse triggers pupation, defined by eversion of the adult head, marking the prepupal–pupal transition. Pupal development continues for several days accompanied by a high ecdysone titer, resulting in terminal differentiation of the adult fly.

Detailed anatomical and histological studies have revealed many biological changes that occur within the puparium in response to these sequential pulses of ecdysone (Bodenstein, 1965; Robertson, 1936). Most larval tissues are destroyed by programmed cell death in a stage-specific manner, while new adult tissues and structures develop from small clusters of progenitor cells. The larval midgut is destroyed in early prepupae as islands of imaginal precursor cells proliferate and fuse to form a new adult gut (Bodenstein, 1965; Jiang et al., 1997). The salivary glands are also destroyed, but not until after the prepupal ecdysone pulse, replaced by an adult salivary gland that differentiates from an imaginal ring of cells at the anterior end of the gland (Robertson, 1936). Salivary gland death occurs by autophagy, with DNA fragmentation, formation of autophagic vacuoles, and caspase activation (Lee and Baehrecke, 2001). The larval muscles are also destroyed in a stage-specific manner, with most anterior muscles destroyed in prepupae and most abdominal muscles destroyed after head eversion (Robertson, 1936). The residual larval muscles act as templates for the formation of adult muscles during pupal development (Bate, 1993; Bodenstein, 1965). Major contractions by the abdominal muscles play a key role in driving the morphogenetic events that accompany pupation (Chadfield and Sparrow, 1985; Robertson, 1936).

Sequential pulses of ecdysone are also critical for proper morphogenesis of the adult appendages from the leg and wing imaginal discs (Fristrom and Fristrom, 1993). These epithelial sheets undergo coordinated changes in cell shape during prepupal development in the absence of proliferation, resulting in initial elongation and eversion of the appendages (Condic et al., 1991; von Kalm et al., 1995). Extensive studies have shown that the late larval ecdysone pulse is required for leg disc elongation and eversion, and the subsequent decrease in ecdysone titer in mid-prepupae is required for pupal cuticle deposition (Fristrom and Fristrom, 1993). Final elongation and differentiation of the legs and wings is then driven by the prepupal and pupal pulses of ecdysone.

Ecdysone exerts its effects on development via hormone-triggered regulatory cascades (Richards, 1997; Russell and Ashburner, 1996; Thummel, 1996). A number of ecdysone-inducible regulatory genes play a key role in controlling larval tissue cell death and/or the formation of adult structures, including the *Broad-Complex (BR-C)* and *crooked legs (crol)*. The *BR-C* encodes a family of zinc finger pro-

teins that function as transcription factors, and is genetically defined by three lethal complementation groups (DiBello et al., 1991; Kiss et al., 1988). The br^+ (*broad*) and $2Bc^+$ functions are required for imaginal disc evagination and fusion, respectively. The rbp^+ (*reduced bristles on palpus*) function is necessary for the destruction of the larval salivary gland and for the development of specific adult thoracic muscles (Restifo and White, 1992). *crol* encodes at least three zinc finger protein isoforms and *crol* mutants die during pupal development with defects in head eversion and leg morphogenesis (D'Avino and Thummel, 1998).

A major impediment in our understanding of insect metamorphosis has been the difficulty in visualizing changes that occur within the intact puparium. As a result, past researchers have depended on either histological sections or whole-mount analysis of dissected tissues from staged animals. These static images do not convey the speed or coordination of developmental responses to ecdysone during metamorphosis. In addition, more subtle morphogenetic changes may escape detection by these methods. Finally, a means of visualizing specific responses to ecdysone, such as leg formation or salivary gland cell death, would allow us to easily identify defects in these pathways in mutant animals.

Here we describe the use of GFP as a marker to follow the fate of the larval salivary glands, larval muscles, and imaginal discs in intact living animals during the onset of metamorphosis. We show that this system can be used to observe the dynamics of larval tissue cell death as well as the formation of the basic body plan of the adult insect. We also show that this system can be used in different mutant backgrounds to study how specific mutant phenotypes arise in ecdysone-triggered developmental pathways.

Materials and methods

Drosophila strains

Fly stocks were maintained at room temperature on standard cornmeal molasses medium. 34B-GAL4 (P{GawB}34B) is on the second chromosome and was used to express GFP in the larval salivary glands (Bloomington stock no. 1967). 24B-GAL4 (P{GawB}how^{24B}) is on the third chromosome and was used to express GFP in the larval muscles (Bloomington stock no. 1767). *Dll*-GAL4 (P{GawB}Dll^{md23}) is on the second chromosome and was used to express GFP in the distal portion of the imaginal discs and adult appendages (Bloomington stock no. 3038). The *Dll*-GAL4 and 24B-GAL4 drivers also show some expression in the larval salivary glands. Two UAS-GFP reporter stocks were used: P{UAS-GFP.S65T}T2 (Bloomington stock no. 1521) and P{UAS-GFP.S65T}T10 (Bloomington stock no. 1522). For GFP studies in mutant animals, GAL4 drivers and GFP reporters were introduced into different mutant backgrounds using appropriate crosses. $crol^3$ is a strong hypomorphic

allele (D'Avino and Thummel, 2000). The *Dll*-GAL4 driver was recombined onto the *crol³* chromosome for visualizing imaginal discs in a *crol* mutant background. *br⁵* is a null allele and *rbp⁵* is a strong hypomorphic allele for these two lethal complementation groups of the *BR-C* (Belyaeva et al., 1980, 1982; Kiss et al., 1988).

Imaging of GFP expression in living animals

Late third instar larvae were selected from the appropriate crosses and monitored every 10–15 min for pupariation. A wild-type animal (usually mutant allele/balancer) was selected for each mutant study at the same stage of development to provide an internal control for developmental timing. Movies of muscle and imaginal discs were started at an early prepupal stage, while salivary gland movies were started in late prepupae. Because salivary gland glue can give background fluorescence, a moist paintbrush was used to remove the glue from the surface of the animal before positioning it for microscopy. Staged prepupae were placed on a glass microscope slide covered with a piece of white or black filter paper. The slide was placed in a humid chamber to maintain viability. This chamber was comprised of a glass petri dish containing an elevated glass slide supported by glass blocks. Water was added to the bottom of the petri dish and filter paper strips were used to wick water from the bottom of the chamber to the slide. The chamber was covered with a plastic petri dish cover with a 2-cm hole bored in the middle, directly over the animals. Animals were maintained at ambient temperature in the room, 22–27°C. Head eversion occurred at 11–13 h after puparium formation in wild-type animals and was delayed by several hours in mutants, as described previously (D'Avino and Thummel, 1998; Karim et al., 1993).

A Zeiss Axiophot microscope modified for digital imaging was used to capture epifluorescence time-lapse images of animals expressing GFP in Figs. 1–4, 6, and 7. The modifications included stage (X–Y) and focus (Z) controls, shutter control, filter wheel, a SensiCamQE high-performance digital CCD camera, and Slidebook 3.0 on a Macintosh G4 computer. Time-lapse images were captured using the following parameters: 2.5×/0.075 Plan-neofluar objective, UV light (528 nm), 2 × 2 binning (640 × 512 pixels final), 300- to 2500-ms exposures (images of mutants that carry only one copy of the transgenes required longer exposure times), 50–300 time points at 10- or 20-min intervals. For salivary gland movies, we used multipoint visitation to simultaneously capture images from multiple animals. For muscle movies, we used a 4D capture protocol to obtain several focal planes, from which one was selected to generate the movies (3–6 Z sections at 50 μm steps for each time point). Long-term exposure (>2 days) to brief bursts of UV light had no apparent effect on viability or development.

A Zeiss Axioplan microscope attached to a Bio-Rad MRC1024 confocal laser was used to image GFP expression in imaginal discs in Figs. 5 and 8, using a Zeiss 2.5× objective. An argon laser was used with excitation at 488 nm and emission at 527 nm. Using the equation $R_d = 1.4n_0\lambda/NA^2$, where *Rd* is the depth resolution (in nm), n_0 is the refractive index of the medium (1.0), λ is the excitation wavelength, and *NA* is the numerical aperture of the lens (0.075), we calculate that the depth resolution of our scans is approximately 0.12 mm. This would cover approximately 15% of the depth of a pupa, which is less than 1 mm in diameter. Laser power was set at 10% and images were captured with Kalman averaging $N = 2$. An automated timed series of images were collected using either 600-s (10 min) or 900-s (15-min) intervals for a total of 71–121 images. The laser scans had no effect on the development of wild-type animals, all of which eclosed normally. The box size for each collection was set to 640 × 480 to have the images in NTSC format, ready for video transfer. The images were stored on a OS/2 driven Dell 2300 computer.

Image processing and video transfer

Images from the digital camera on the Axiophot were exported from SlideBook 3.0 as a series of individual TIFF files. Each TIFF file in a sequence was adjusted, and times were added (h:min), using Adobe Photoshop. These modified images were imported into Adobe Premier and exported as a QuickTime movie. Images from the confocal microscope were exported using Bio-Rad LaserSharp processing software as a series of individual Apple PICT files. Text depicting the time (h:min) was added to each image and the Video:NTSC color filter was used to prepare each image for video, using Adobe Photoshop. This series was imported into Adobe Premier and exported as a QuickTime movie. Selected images from each movie were used to generate the figures in Adobe Photoshop.

Results

Destruction of the larval salivary glands and muscles in early pupae

The 34B-GAL4 driver was used to express GFP in the larval salivary glands. Animals were collected as newly formed prepupae, aged for 6–9 h at 25°C, and images were collected at 10-min intervals until 21–25 h after puparium formation. In the experiment shown in Fig. 1A, the large lobes of the larval salivary glands can be easily visualized along the ventral surface of the animal prior to head eversion (12:00). The glands contract slightly, then rapidly move toward the dorsal region of the animal as the head everts, with only the most anterior portion of the gland remaining in focus. GFP fluorescence gradually diminishes with only a faint signal visible by ~8 h after head eversion (20:00). A lateral view of the salivary glands, shown in Fig. 1B, more clearly illustrates the sudden movement of the
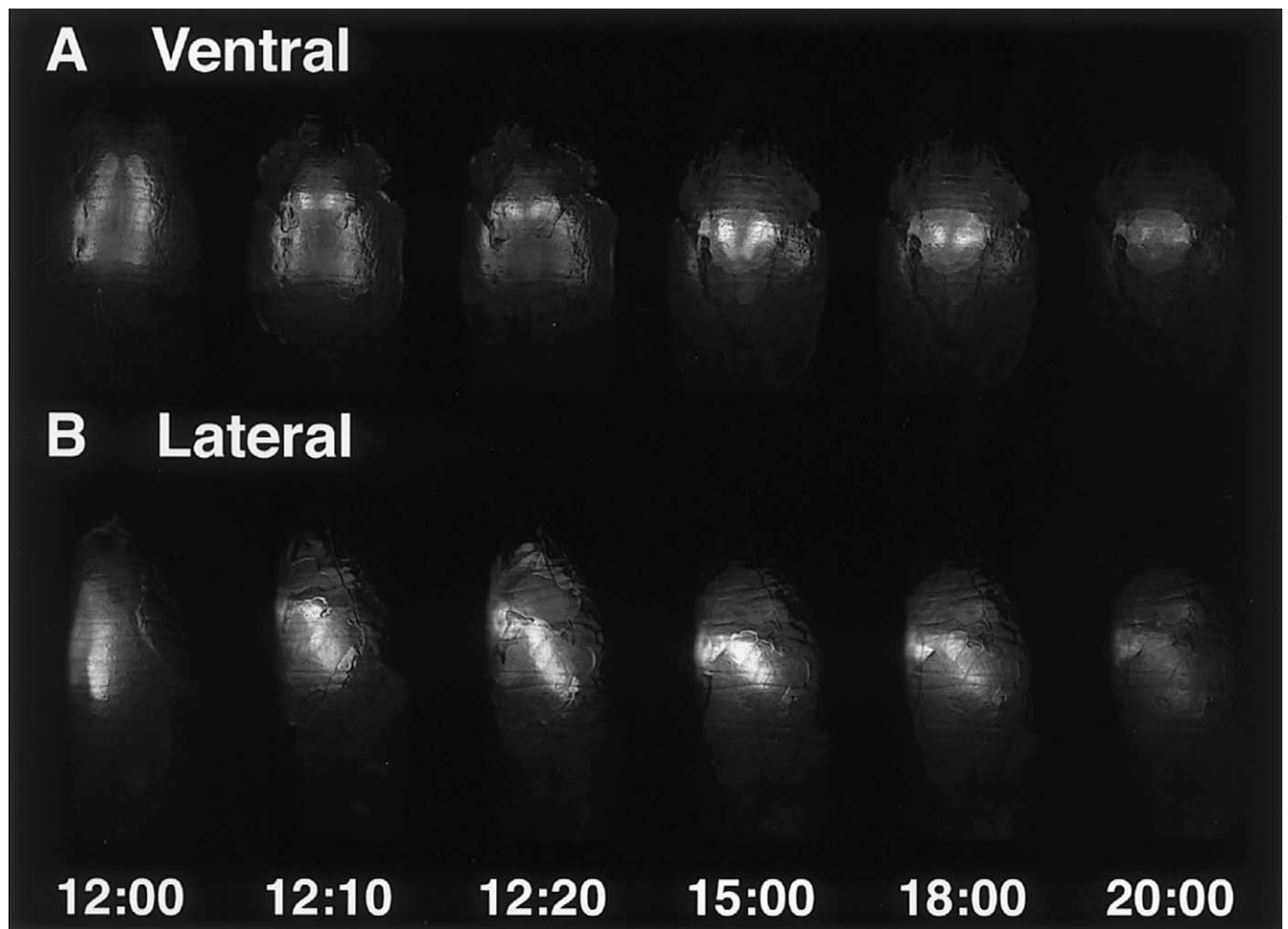
Fig. 1. Translocation and destruction of the larval salivary glands in early pupae. Images were collected at 10-min intervals from either (A) the ventral side or (B) the lateral side of a late prepupa that carries the 34B-GAL4 driver and UAS-GFP reporter. These images were compiled into time-lapse movies that can be seen as Online supplementary data. Representative images from these movies are depicted. The times are normalized such that 12:00 is 10 min prior to adult head eversion.

salivary glands toward the dorsal aspect of the animal at head eversion. This is followed by a slight contraction and gradual dissolution of the glands. See Online supplementary data for Quicktime movies of Fig. 1A and Fig. 1B. Similar responses were observed in six different animals.

The larval muscles in the abdomen have been reported to be destroyed in synchrony with the salivary glands, in early pupae (Robertson, 1936). To visualize this response, the 24B-GAL4 driver was used to express GFP in the larval muscles, and images were collected at 20-min intervals through prepupal and early pupal development. The characteristic array of larval muscles can be seen in the prepupal abdomen (Fig. 2, 2:00, 10:00). The muscles begin to break up and become disorganized about 2 h before head eversion (Fig. 2, see boxed region in 10:00–12:00). Muscles are still evident at early times after head eversion (Fig. 2, 12:20, 12:40), followed by their rapid dissolution until the individual muscles are no longer seen (Fig. 2, 14:20, 16:20). See

Online supplementary data for a Quicktime movie of Fig. 2. Similar responses were observed in three different animals.

We also attempted to visualize the destruction of the anterior larval muscles in these animals, which occurs during the first half of prepupal development (Robertson, 1936). Clear images of these muscles, however, could not be obtained, despite numerous attempts. One reason for this is that the 24B-GAL4 driver, as well as e22c-GAL4 and rp298-GAL4 (Menon and Chia, 2001), all of which are muscle-specific in embryos, gave more nonspecific GFP expression in prepupae. It was thus difficult to detect the larval muscles above the background fluorescence. This was compounded by the contraction of the early prepupa which occurs shortly after puparium formation, shifting the anterior larval muscles into a wide range of focal planes. In contrast, the abdominal larval muscles, as viewed from the ventral surface, remain within a relatively narrow focal plane and thus can be readily visualized as they progress through cell death (Fig. 2).
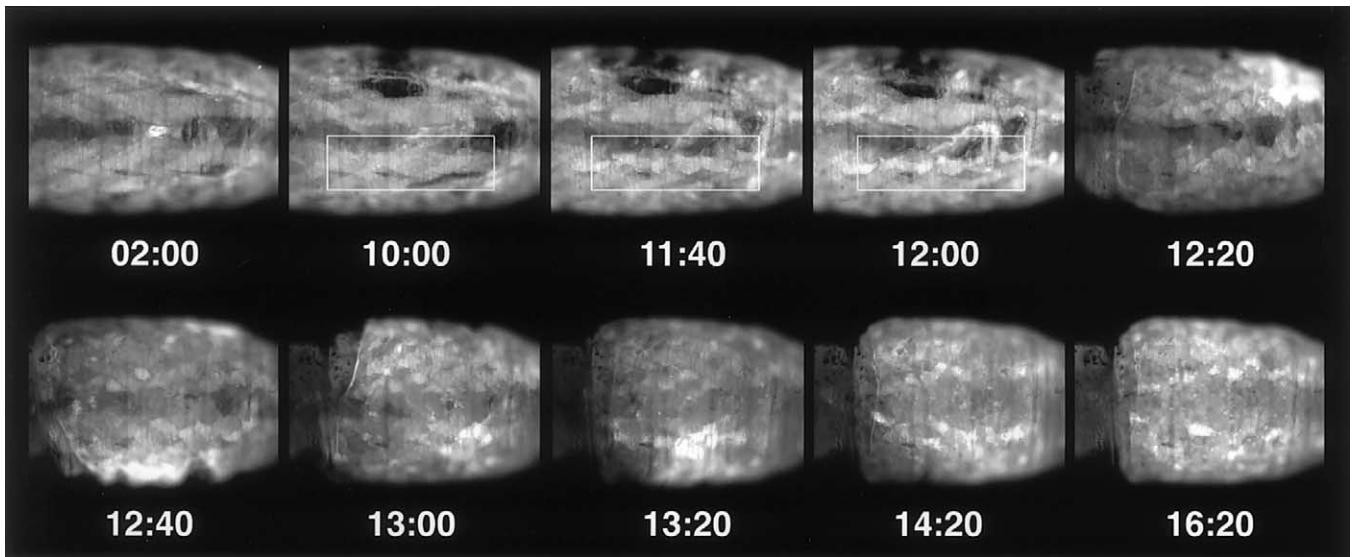
Fig. 2. Destruction of the larval abdominal muscles. Images were collected at 20-min intervals from the ventral side of a 2-h prepupa that carries the 24B-GAL4 driver and UAS-GFP reporter. A z-series stack of six images was collected for each time point and one section was selected from each stack to create the time-lapse movie in Online supplementary data. Representative images from this movie are depicted, with the corresponding times shown below in hours:minutes. The boxed region highlights larval muscles that degenerate prior to head eversion.

Larval salivary glands and muscles fail to die in rbp[5] mutants

To determine how effectively the GAL4/GFP system could be used to analyze defects in the destruction of larval tissues during metamorphosis, we followed the fate of the larval salivary glands and abdominal muscles in *rbp[5]* mutants of the *BR-C*. Although these mutants display a high penetrance of salivary gland cell death defects, the effects of this mutation on larval muscle cell death have not been reported (Jiang et al., 2000; Restifo and White, 1992; Zhimulev et al., 1995).

The 34B-GAL4 driver and UAS-GFP responder were introduced into an *rbp[5]* mutant background to follow salivary gland cell fate. Images were collected at 10-min intervals from mutant late prepupae until ~9 h after head ever-
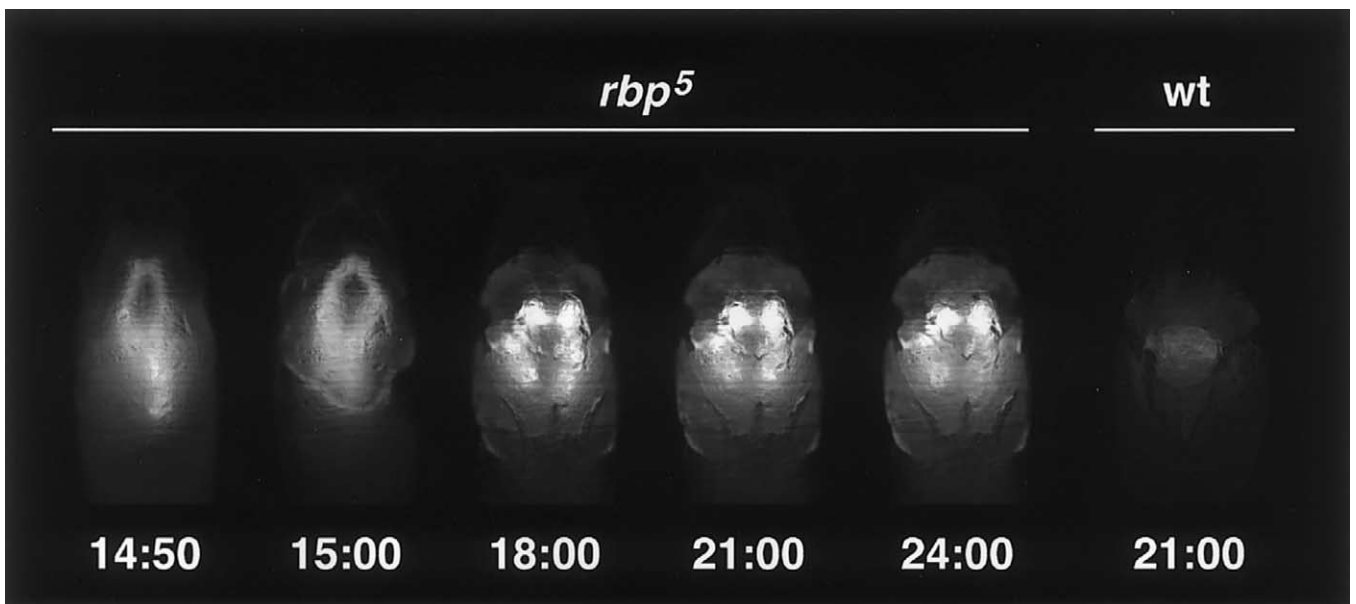

Fig. 3. Salivary glands fail to die in *rbp[5]* mutants. Images were collected at 10-min intervals from the ventral side of a 12-h *y rbp[5] w[a] sn[3]*/Y; 34B-GAL4, UAS-GFP (1521)/+ prepupa. These were compiled into a time-lapse movie that can be seen as Online supplementary data. Representative images from this movie are depicted. A control wild-type pupa is shown on the right (wt) for comparison. Head eversion is delayed by ~3 h in the *rbp[5]* mutant prepupa relative to the wild-type, thus the wild-type 21:00 image is equivalent in developmental time to the 24:00 mutant timepoint.
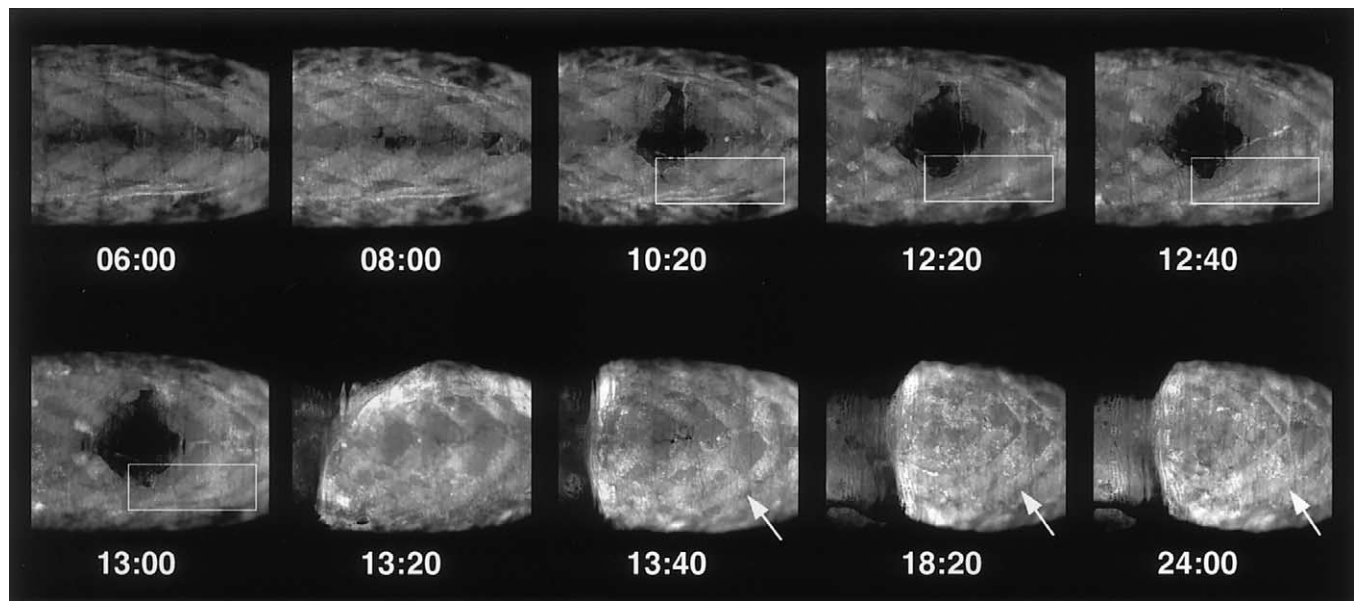
Fig. 4. Muscles fail to die in rbp^5 mutants. Images were collected at 20-min intervals from the ventral side of a 6-h y rbp^5 w^a sn^3/Y; UAS-GFP (1521)/+; 24B-GAL4/+ prepupa. These were compiled into a time-lapse movie that can be seen as Online supplementary data. Representative images from this movie are depicted. The boxed region highlights larval muscles that fail to degenerate as they would in a wild-type prepupa (see Fig. 2). The arrows mark one of the persistent abdominal muscles.

sion. Fig. 3 shows that the larval salivary glands look normal during prepupal development, with one gland moving on top of the other in this animal (14:50). The glands then dive at head eversion but do not fall apart and there is little, if any, reduction in GFP fluorescence throughout the time course (Fig. 3, 24:00). In contrast, a control wild-type animal shows only a low level of residual fluorescence from the salivary glands (Fig. 3, wt 21:00). GFP expression can still be detected in the mutants several days after head eversion (data not shown). See Online supplementary data for a Quicktime movie of Fig. 3. A similar phenotype was observed in dozens of rbp^5 mutant animals.

The 24B-GAL4 driver and UAS-GFP responder were crossed into an rbp^5 mutant background to follow abdominal muscle cell fate. Images were collected at 20-min intervals from mutant animals, starting at 2–8 h and ending at 24–28 h after puparium formation. Fig. 4 shows the normal array of abdominal muscles in an rbp^5 mutant prepupa, with a prominent gas bubble appearing after 09:00. The muscle degeneration that is apparent ~2 h before head eversion in wild-type prepupae is not seen in the rbp^5 mutant animals (Figs. 2 and 4, boxed regions), although the muscles appear less organized than at earlier stages. Similarly, intact muscles can be seen after head eversion in rbp^5 mutant pupae, more than 1 day after puparium formation (Fig. 4, arrows). Significant muscle contractions are apparent in early rbp^5 mutant pupae, starting at head eversion (13:20 in the animal in Fig. 4) and continuing for as long as 5 h, consistent with the ability of the persistent muscles to remain active. Muscle contractions in wild-type animals are only evident for 2.7–3.0 h after head eversion ($n = 5$). See Online supplementary

data for a Quicktime movie of Fig. 4. Similar phenotypes were observed in five different rbp^5 mutant animals.

The imaginal discs undergo rapid and coordinate morphogenesis

We used *Dll*-GAL4 to drive GFP expression in the imaginal discs of newly formed prepupae as a first step toward observing the dynamics of adult tissue development during metamorphosis. Images were collected from wild-type animals at 15-min intervals through prepupal and early pupal development and compiled to form a movie. As viewed from a ventral perspective, the legs become visible in a reproducible order as they elongate within the puparium. The second pair of legs (T2 legs) are already elongated and visible in a newly formed prepupa (Fig. 5, 00:00). The first (T1) and third (T3) pair of legs elongate in synchrony with the second pair; however, the T1 legs are initially buried underneath the T2 legs and the T3 legs are located laterally. The T1 legs move in an anterior direction, out from underneath the T2 legs, and become visible between 03:00 and 04:00 (Fig. 5). One leg in each pair often overlaps the other at first and then moves laterally to assume its normal position next to the other (this can be seen for the T2 legs in Fig. 5, 00:00 and 03:00). The third pair of legs come into view last, between 04:30 and 06:00, moving from their initial lateral location toward the ventral region of the animal. Starting at 05:00, the legs bend back upon themselves as they begin the process of eversion. The legs then fold back further and evert rapidly, moving outside the puparium between 05:30 and 05:45. The wings elongate laterally and
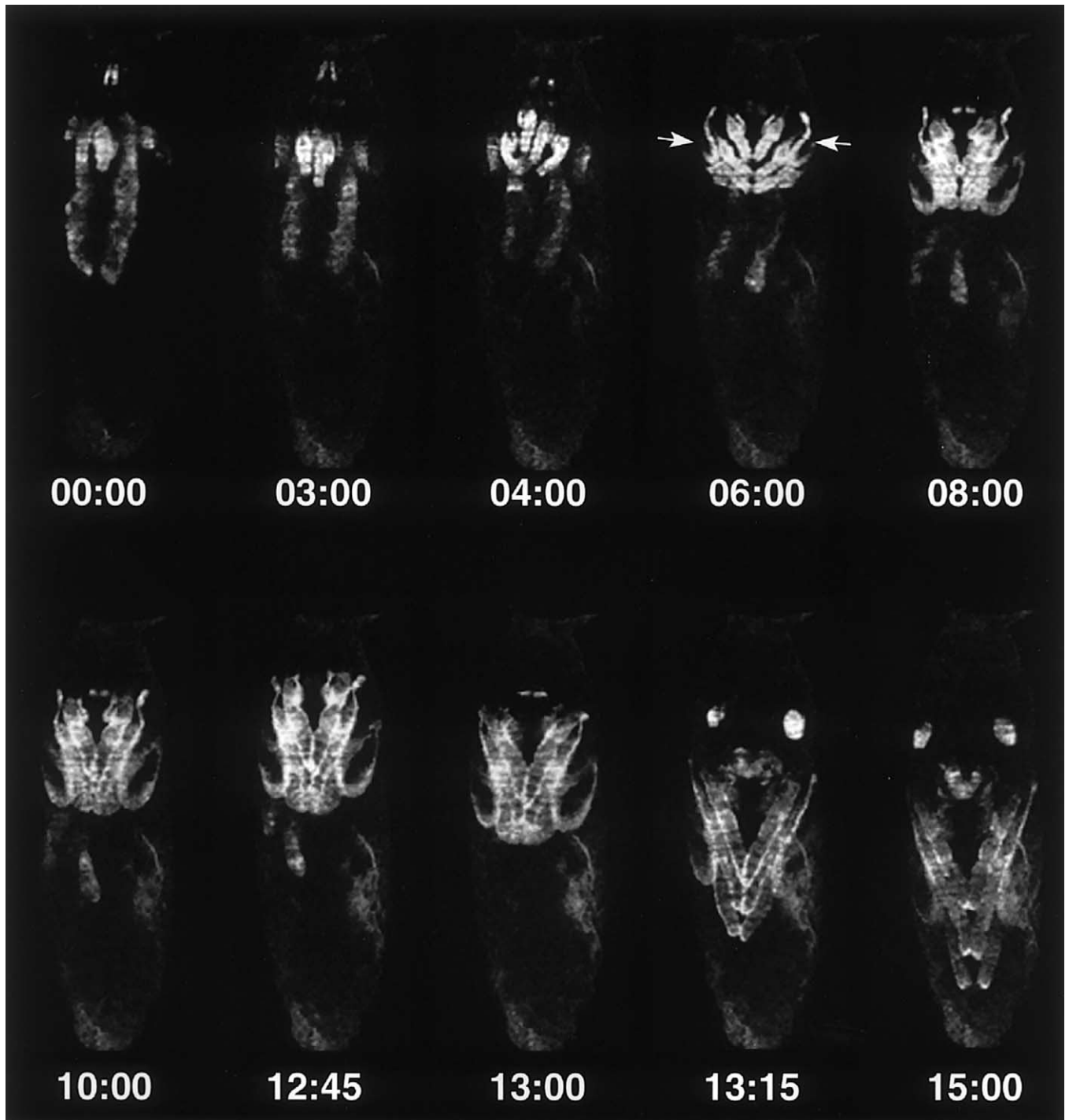
Fig. 5. Imaginal disc morphogenesis and head eversion establish the basic body plan of the adult fly. Images were collected at 15-min intervals from the ventral side of a 0-h prepupa that carries the *Dll*-GAL4 driver and UAS-GFP reporter. These images were compiled into a time-lapse movie that can be seen as Online supplementary data. Representative images from this movie are depicted, with the corresponding times shown below in hours:minutes. The arrows at 06:00 mark the everted wings. Salivary glands can be seen throughout most of prepupal development.

first become visible, from a ventral perspective, between 05:00 and 06:00 (Fig. 5, 06:00, arrows). The legs do not appear to undergo further elongation between 06:00 and 09:00 and form an ordered regular array along the ventral surface of the animal. The wings continue to elongate along the lateral sides of the animal between 06:00 and 08:00.

From 09:00 to 10:30, the legs undergo a second, more minor, step in their elongation. Head eversion occurs between 13:00 and 13:15 in Fig. 5. The eye-antennal imaginal discs rapidly rotate out to the sides of the everting adult head as the mouthparts begin to form (Fig. 5, 13:00, 13:15). In addition, the legs straighten and, together with the wings,

undergo a final significant elongation between 13:00 and 13:15. By 15:00, the basic body plan of the adult fly has been established (Fig. 5). See Online supplementary data for a Quicktime movie of Fig. 5. Similar responses were observed in dozens of wild-type animals.

We noted an unusual variation that occurred in 14% of wild-type animals (five experiments with sample sizes of 9–29 animals per experiment) where one of the T1 legs moves out on the wrong side of a T2 leg shortly after puparium formation. This can be seen in a second movie of wild-type animals where images were captured at 10-min intervals from 00:00 to 50:00 h relative to puparium formation (Fig. 6). As the T1 legs begin to move out in an anterior direction from underneath the T2 legs, one of the T1 legs moves out on the wrong side of its corresponding T2 leg (Fig. 6, 03:30, arrow), rather than between the pair of T2 legs as is seen in the majority of wild-type animals (Fig. 5, 04:00). The T1 leg then moves back underneath the T2 leg to assume its appropriate location next to its partner (Fig. 6, 04:20–05:00, arrow). This movement is always complete immediately before disc eversion, which occurs at 05:10–05:20 in this animal.

Continuing this movie from head eversion until 50 h after puparium formation reveals remarkable refinement of the imaginal disc-derived adult cuticular structures. *Dll* expression in the eye-antennal disc marks only the antennal portion, revealing a slow migration of these structures from an initial lateral position on the head to their appropriate final location at the anterior end of the puparium by ~12 h after head eversion (Fig. 6, 11:00–23:30). This movement has not, to our knowledge, been reported previously. As the antennal discs complete their migration, the legs reveal their segmented structure. This continues through the end of the time course, as the mouthparts become refined. Folds can also be seen to form within the developing wings during the final ~10 h of the time course (Fig. 6, arrows, 41:00–47:10). See Online supplementary data for a Quicktime movie of Fig. 6. Similar responses were observed in three wild-type animals.

br⁵ and crol³ mutants display defective adult leg morphogenesis

Earlier studies have shown that br^5 and $crol^3$ mutations result in leg malformations that can be detected during prepupal and early pupal development (Kiss et al., 1988; D'Avino and Thummel, 1998). We have examined the origin of these phenotypes in living animals using the *Dll*-GAL4 driver and UAS-GFP reporter in br^5 and $crol^3$ mutant backgrounds (Figs. 7 and 8). In agreement with earlier studies (Kiss et al., 1988), the br^5 mutation results in a complete block in leg morphogenesis, with no eversion or elongation (Fig. 7). The leg discs move around slowly in these animals, but show no developmental changes. These animals undergo a series of contractions beginning at 16:00 and increasing in intensity between 18:00 and 19:00 that appear to reflect an attempt at head eversion. One leg imaginal disc is often forced away from the others by these

contractions (Fig. 7, 18:00–19:00). Similar strain variations have been reported in the timing of the prepupal ecdysone pulse that triggers these muscle contractions (Richards, 1981). See Online supplementary data for a Quicktime movie of Fig. 7. Similar responses were observed in five different movies generated from this genotype.

$crol^3$ mutants also display defects in leg disc morphogenesis (Fig. 8). The T1 and T2 legs appear at the proper times relative to wild-type. Interestingly, however, all four $crol^3$ mutants examined revealed initial mislocalization of one T1 leg, as reported above for a minority of wild-type prepupae (Fig. 8, 02:50–03:50, arrow). Figure 8 represents the least severe mutant examined; the other three $crol^3$ mutants more closely displayed the degree of T1 movement depicted in Fig. 6. The T2 legs begin to fold at 04:30. The T3 legs appear between 05:40 and 08:00, as the legs evert to the outside, revealing a 1 to 2-h delay in disc eversion relative to wild-type. $crol^3$ mutant legs also fail to form the clearly ordered array that is evident upon completion of eversion in wild-type prepupae and they undergo no significant elongation after 08:00 (Fig. 8). As a result, the final leg elongation that occurs at head eversion, which is delayed in $crol^3$ mutants to between 15:30 and 16:00 (Fig. 8), results in legs that are significantly shorter than those seen in wild-type pupae (Fig. 8, 20:00, arrow). The legs are also malformed at this stage, with one of the third legs wrapped around the edge of the wing (Fig. 8, 20:00, arrowhead) (see also Fig. 2B, D'Avino and Thummel, 1998). See Online supplementary data for a Quicktime movie of Fig. 8. Similar responses were observed in four $crol^3$ mutant animals.

Discussion

The past 15 years have seen major strides forward in our understanding of the genetic regulation of *Drosophila* embryogenesis and pattern formation. In contrast, our understanding of metamorphosis remains relatively poor. In large part, this disparity can be attributed to our inability to see the remarkable morphogenetic changes that occur within the puparium. Here, we show that tissue-specific expression of GFP can be used to follow the fates of different tissues in living animals during the early stages of *Drosophila* metamorphosis. We have also used this method to gain insight into the origin of lethal phenotypes associated with mutations in ecdysone-inducible regulatory genes. This approach provides a new means of studying the temporal coordination of key developmental events associated with insect metamorphosis.

Visualization of larval salivary gland and muscle cell death during metamorphosis

Prior to this report, our understanding of larval salivary gland cell death was derived from end-point analysis, by either dissecting or sectioning staged pupae. These studies
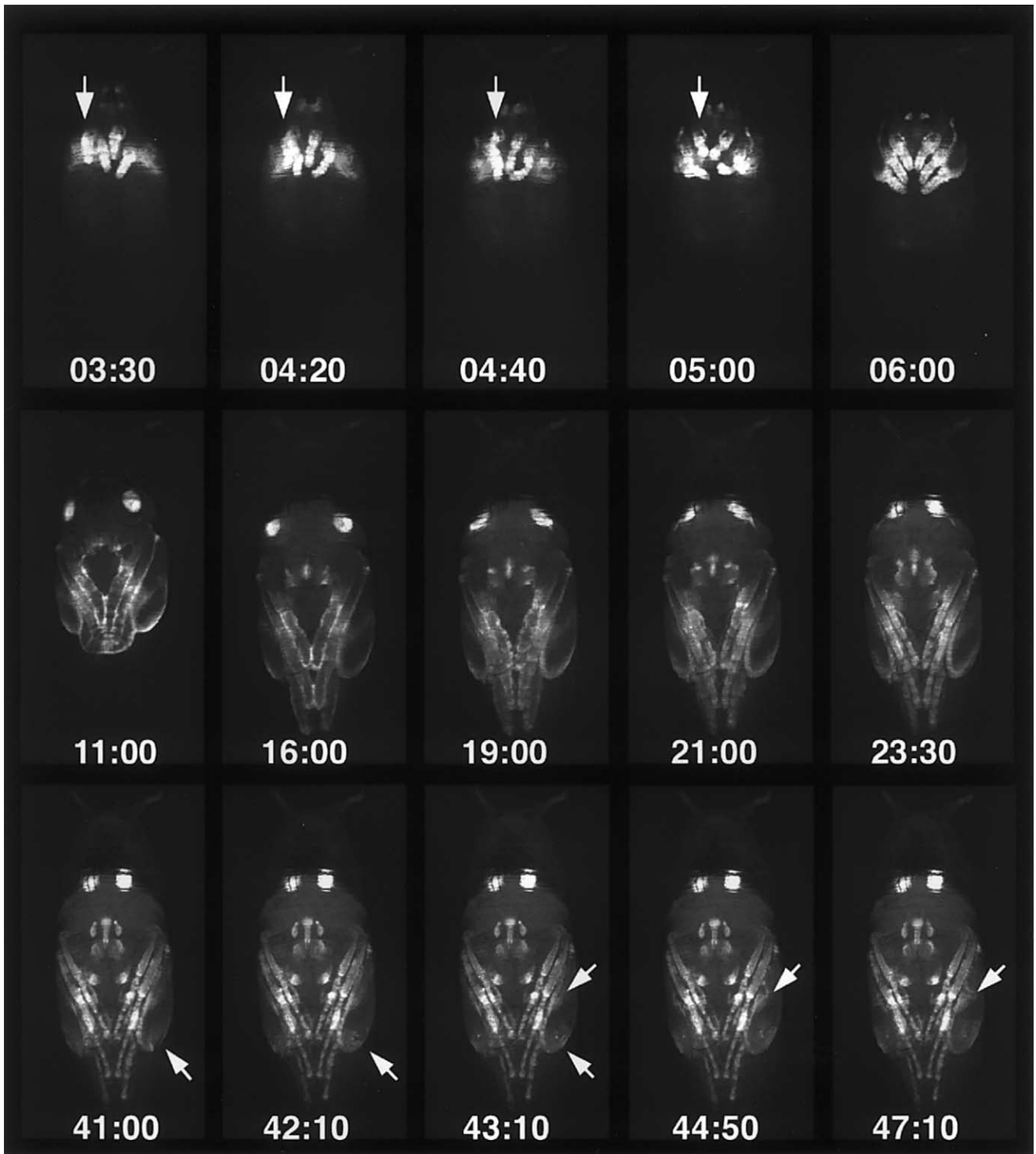
Fig. 6. Movement of a T1 leg in an early prepupa and pupal morphogenetic events. Images were collected at 10-min intervals from the ventral side of a 0-h prepupa that carries the *Dll*-GAL4 driver and UAS-GFP reporter. These images were compiled into a time-lapse movie that can be seen as Online supplementary data. Representative images from this movie are depicted, with the corresponding times shown below in hours:minutes. The arrows at 03:10–05:00 mark the movement of a T1 leg to its appropriate location between the T2 pair of legs. The arrows at 41:00–47:10 mark the folds that form in the wing.

described rapid degeneration of the salivary glands between 14.5 and 15.5 h after puparium formation (Jiang et al., 1997; Lee and Baehrecke, 2001; Robertson, 1936). In contrast, our

imaging shows a gradual reduction in GFP fluorescence after the glands shift away from the ventral surface of the animal at head eversion, with signal still evident several
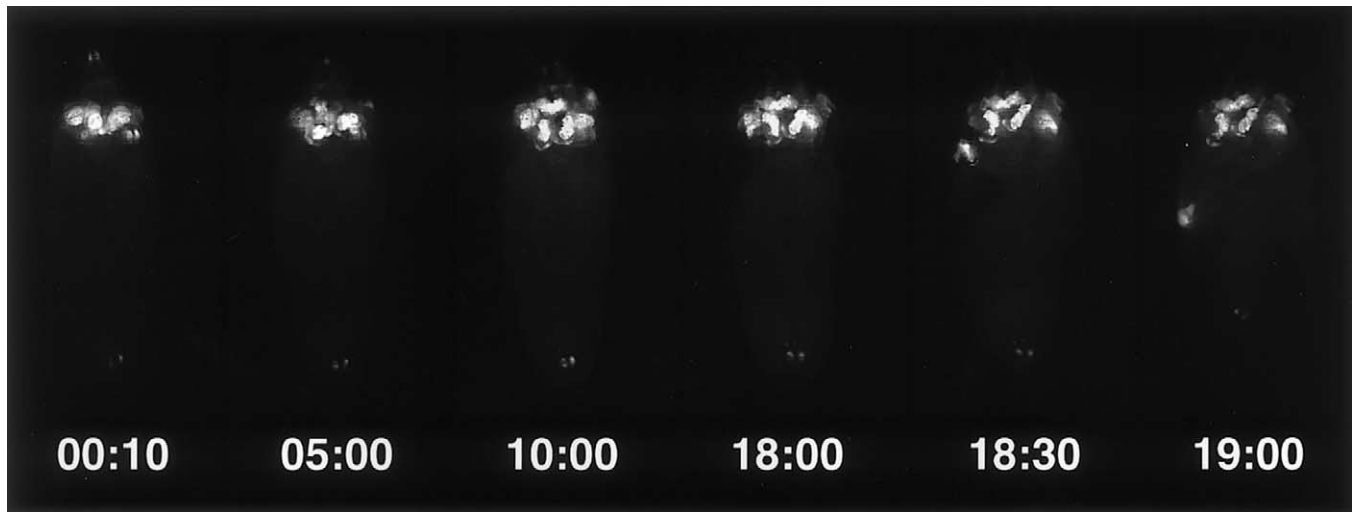
Fig. 7. br^5 mutants display no eversion or elongation of leg imaginal discs. Images were collected at 10-min intervals from the ventral side of a 0-h y br^5/Y; *Dll*-GAL4/UAS-GFP (1521) prepupa. These images were compiled into a time-lapse movie that can be seen as Online supplementary data. Representative images from this movie are depicted, with the corresponding times shown below in hours:minutes.

hours after the glands can no longer be dissected (Fig. 1, 18:00). It is not until ~20 h after puparium formation when GFP levels become significantly reduced. It is likely that this gradual decrease in signal derives from GFP protein that is slowly degraded within the dying salivary gland. Dissection of staged pupae revealed that the GFP-expressing salivary glands fall apart when removed from animals older than ~16 h after puparium formation. Thus, the GFP fluorescence marks the remnants of this tissue within the animal, allowing us to visualize them at later stages than

otherwise possible. Our imaging also reveals a dramatic translocation of the salivary glands toward the dorsal region of the animal at head eversion, a movement that has not been described previously and that would be difficult to see with other methods of analysis. It is likely that this translocation is a passive response to the major movements that accompany adult head eversion.

Larval muscle cell death has not been studied as extensively as that of the salivary glands because it is so difficult to visualize. The muscles can only be seen in sections or by
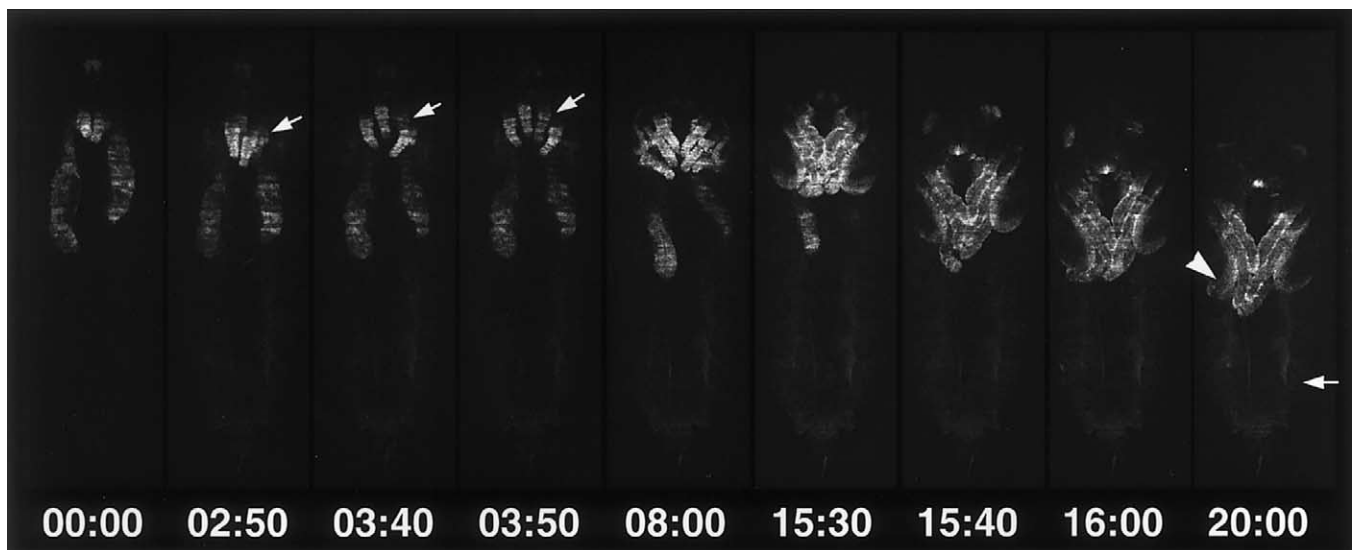

Fig. 8. $crol^3$ mutants display defects in adult leg morphogenesis. Images were collected at 10-min intervals from the ventral side of 0-h y w; *Dll*-GAL4 $crol^3$/Df(2L)esc^{10}; +/UAS-GFP (1522) prepupa. These images were compiled into a time-lapse movie that can be seen as Online supplementary data. Representative images from this movie are depicted, with the corresponding times shown below in hours:minutes. Salivary glands can be seen throughout most of prepupal development in this genetic background. The arrows in 02:50, 03:40, and 03:50 mark a T1 leg that has everted in an improper position. The arrowhead in panel 20:00 marks a malformed third leg that is wrapped around the edge of the wing, while the arrow marks the approximate extent of final leg elongation in wild-type animals.

carefully opening the pupal case that surrounds the puparium. The GAL4/GFP system allows us, for the first time, to follow the dynamics of larval muscle cell death in a living animal. Our observations correspond well with earlier studies. As described by Crossley (1978), the abdominal muscles are "decimated" beginning at pupation. Robertson (1936) reports that these muscles show distinct signs of degeneration immediately after pupation, with many broken up within the body cavity by 2 h later. This agrees with the rapid breakdown of muscles that we see immediately after head eversion (Fig. 2). In addition, we see clear indications of a loss of abdominal muscle integrity starting approximately 2 h before head eversion (Fig. 2, boxes). The long muscles begin to fragment and break apart during this time. This was not reported in earlier studies, although Robertson (1936) refers to "slight liquifaction" of the doomed abdominal muscles during prepupal stages.

The abdominal muscles must still be capable of exerting significant force at pupation, despite their partial degeneration. Rhythmic contractions by the abdominal muscles move a gas bubble that forms in mid-prepupae toward the posterior end of the animal and then along the sides to the anterior end (Chadfield and Sparrow, 1985; Robertson, 1936). This translocation pushes the animal to the posterior region of the puparium, providing space at the anterior end for the future adult head. Major muscle contractions then force the head to evert from within the thoracic sac, to occupy its final location at the anterior end of the animal. Several studies have concluded that this morphogenetic movement is driven by hydrostatic pressure, caused by the abdominal muscles forcing hemolymph into the developing head capsule (Bodenstein, 1965; Chadfield and Sparrow, 1985; Robertson, 1936; Wahl, 1914). Immediately after these contractions, the abdominal muscles die.

We also examined the effects of the *BR-C rbp⁵* mutation on larval muscle and salivary gland cell death. Consistent with earlier studies (Jiang et al., 2000; Restifo and White, 1992; Zhimulev et al., 1995), the salivary glands fail to die in *rbp⁵* mutants (Fig. 3). Similarly, degeneration of the abdominal muscles that is apparent immediately before head eversion in wild-type animals is not seen in *rbp⁵* mutants (Figs. 2 and 4, boxed regions), and intact larval muscles that extend along the abdomen can be detected beyond 24 h after puparium formation (Fig. 4, arrows), a phenotype that is never observed in wild-type animals. Interestingly, the persistent abdominal muscles in *rbp⁵* mutant pupae continue to contract for up to 5 h after head eversion, indicating that they remain functional. This observation also suggests that the rapid disintegration of wild-type abdominal muscles immediately after head eversion may be a consequence of their self-destruction, with the muscles tearing themselves apart as their cells undergo programmed cell death. We conclude that the *BR-C* plays a critical role in larval abdominal muscle cell death during metamorphosis.

Ecdysone pulses coordinate major morphogenetic changes that form the basic body plan of the adult fly

Our studies reveal a remarkable series of rapid and coordinated morphogenetic responses to the late larval and prepupal pulses of ecdysone. The legs can be followed during their elongation, initially within the puparium and later everting to the outside where they undergo final stages of elongation and differentiation. The overlapping T1 and T2 legs that we see in early wild-type prepupae as well as the movement of the T1 legs relative to the T2 legs have not been reported previously, revealing the dynamics of imaginal disc morphogenesis triggered by the late larval pulse of ecdysone. It is important to note that this movement represents only the distal portion of the leg, reflecting the pattern of *Dll*-GAL4 expression in the tarsal and distal tibia of the leg (Cohen, 1993). We assume that the more proximal region of the leg discs are relatively static at this stage, undergoing fusion to form part of the adult thorax (Fristrom and Fristrom, 1993). It should be noted, however, that Usui and Simpson (2000) have reported that wild-type wing imaginal discs move dorsally after eversion, prior to spreading and fusing along the midline. The discs may thus be capable of limited movement, ensuring that they will occupy their appropriate position in the animal prior to their final morphogenesis and differentiation.

We find that leg disc eversion occurs within a 10- to 20-min interval at 5.5–6 h after puparium formation, in agreement with earlier observations (Fristrom and Fristrom, 1993; Robertson, 1936). This is preceded by significant folding of the elongating legs inside the animal, which is evident for 30–45 min before eversion. This most likely arises from the contracting peripodial epithelium which eventually pushes the elongating legs through the disc stalk to the outside of the puparium (Milner et al., 1984). Both leg elongation and peripodial epithelial contraction occur by ecdysone-triggered changes in cell shape which drive morphogenesis (Fristrom and Fristrom, 1993).

The *Dll*-GAL4 driver allows us to follow the dynamics of adult head eversion in an intact living animal. This response occurs immediately after the ecdysone pulse that defines the end of prepupal development, at ~13 h after pupariation in the animal shown in Fig. 5. Head eversion has been reported to occur in less than 15 min (Chadfield and Sparrow, 1985; Robertson, 1936), a time frame that is in close agreement with our observations. The most dramatic manifestation of this response is the rapid translocation of the eye-antennal imaginal discs from their larval position to a lateral location in the adult head. The imaginal discs that comprise the adult head must fuse during prepupal development to allow a unified response to the muscular contractions that drive head eversion. This fusion most likely occurs during mid-prepupal stages, in parallel with fusion of the thoracic imaginal discs (Fristrom and Fristrom, 1993). Following the animal through later stages of pupal

development reveals that the antennae slowly move along the head to assume their final location at the anterior end of the puparium, while the mouthparts are refined (Fig. 6). The legs and wings undergo rapid and dramatic elongation at head eversion, increasing significantly in length, establishing their adult form (Figs. 5 and 6). This process is reported to occur in a manner similar to that of head eversion, in which the discs are inflated by hydrostatic pressure in response to strong abdominal muscle contractions (Fristrom and Fristrom, 1993). The length and form of the final adult structures are then fixed in place by deposition of a rigid cuticle. As a result of these coordinated responses, the animal assumes the basic plan of the adult fly, with a head, thorax, abdomen, wings, and legs. Final differentiation occurs over the ensuing days of pupal development as the legs acquire their adult form and the wings become folded (Fig. 6).

Adult legs fail to evert and elongate normally in br^5 and $crol^3$ mutant prepupae

We have used the *Dll*-GAL4 driver to follow the dynamics of leg imaginal disc morphogenesis in living br^5 and $crol^3$ mutant prepupae (Figs. 7 and 8). Our observations confirm and extend earlier phenotypic studies of these mutants. br^5 mutants display a complete arrest in leg morphogenesis with no signs of eversion or elongation (Fig. 7), consistent with earlier work (Kiss et al., 1988). Unexpectedly, these animals show a series of apparent muscular contractions at ~18 h after pupariation, reflecting an aberrant attempt at head eversion and confirming that the animals are still alive at these later stages (Fig. 7). We also often see one leg imaginal disc aberrantly forced away from the others by these contractions, consistent with the known inability of these discs to fuse properly during prepupal development (Kiss et al., 1988).

$crol^3$ mutants are also characterized by defects in adult leg morphogenesis (D'Avino and Thummel, 1998). Leg discs were dissected from 6-h $crol^3$ mutant prepupae in an effort to understand the origins of this phenotype, revealing that they are often distorted and reduced in length at this early stage in their development (D'Avino and Thummel, 1998). This effect is seen in movies of $crol^3$ mutant prepupae, although we can also discern several other defects in leg morphogenesis. One of the T1 legs moves to the wrong position relative to its corresponding T2 leg in all four $crol^3$ mutants examined, suggesting an increase in the penetrance of this phenotype that is normally seen in only 14% of wild-type animals. $crol^3$ mutant legs also display a 1- to 2-h delay in disc eversion, fail to form an organized array along the ventral surface as is seen in wild-type mid-prepupae, and fail to undergo elongation in late prepupal stages. As a result of these defects, $crol^3$ mutant legs do not straighten or elongate properly at head eversion (Figs. 5 and 8). The movies thus provide a detailed and dynamic understanding of the origins of the leg malformation caused by *crol* mutations.

GAL4-mediated GFP expression provides a new method for observing developmental changes in living animals undergoing metamorphosis

Earlier studies of *Drosophila* metamorphosis have depended on static images obtained by dissecting or sectioning staged prepupae and pupae. In contrast, the automated capture of fluorescent GFP images allows us to follow the dynamics of ecdysone-triggered developmental responses in living animals during metamorphosis. This approach reveals the speed and coordination of these events in both wild-type and mutant genetic backgrounds. For example, the rapid dorsal translocation of the larval salivary glands at head eversion has not been reported previously, most likely because it is difficult to follow the fate of this fragile dying tissue without the noninvasive approach of GFP imaging. Similarly, the *Dll*-GAL4/GFP expression patterns during prepupal and pupal stages dramatically convey the morphogenetic changes that occur as the animal converts its body plan from that of a crawling larva to an adult fly. Although many of these events have been described as early as Robertson's classic study in 1936, some have not. Moreover, the GFP movies reveal the beauty of these responses as well as uncover subtleties that would otherwise be missed.

The noninvasive nature of this method also provides a more accurate characterization of mutant phenotypes than is otherwise possible. For example, although the rbp^5 mutation results in persistent larval salivary glands that can be easily dissected from pupae many hours after head eversion, persistent glands in other mutant backgrounds are often fragile, making them difficult to score. The GAL4/GFP system provides a rapid and simple means of visualizing salivary glands in an intact animal, allowing one to easily score large numbers of animals for salivary gland death defects. Similarly, we have found it difficult to characterize defects in leg morphogenesis during prepupal development by more conventional approaches. Simply dissecting and mounting prepupal leg imaginal discs can often result in malformations, even in wild-type animals (J. Gates, unpublished results). Thus, it has been difficult to determine how a leg malformation that is evident in early pupae might have arisen during prepupal stages. The GAL4/GFP system provides a rapid and simple means of determining the origins of leg malformations, as well as revealing subtle mutant phenotypes such as the asynchrony of leg eversion and translocation of the T1 legs.

Several technical considerations, however, must be kept in mind when using this method. Visualization by confocal microscopy is only useful when a relatively narrow depth of focus is of interest. Thus, for example, the destruction of the larval salivary glands cannot be followed by confocal microscopy because this tissue dives toward the dorsal side of the puparium at head eversion. In contrast, imaginal disc eversion and elongation, which occurs along the ventral surface of the animal, can be clearly visualized under the confocal microscope. In addition, the GAL4 drivers selected

for this method need to be expressed at relatively high levels, particularly when attempting to visualize tissues that lie deep within the body. This allows one to use rapid shutter speeds, minimizing exposure of the animal to UV or laser light and providing sharp images. The drivers also need to be highly tissue specific at the stages of interest, reducing background fluorescence. It will be interesting to expand this study to follow other morphogenetic responses during metamorphosis—for example, dorsal closure of the thorax or histoblast development. Combined with optimized GFP reporters, these drivers could reveal new developmental pathways and dynamic responses that had not been previously detectable.

Finally, the GAL4/GFP system provides a new approach to design genetic screens for defects in specific ecdysone-triggered developmental pathways. Individual tissues can be readily observed in living animals by simply rolling vials under a dissecting microscope equipped to detect GFP fluorescence. For example, we currently have a screen underway using salivary gland-specific GFP expression to score for defects in steroid-triggered programmed cell death (A. Bashirullah, unpublished results). Similar screens could be designed for defects in other ecdysone-regulated developmental responses. Taken together, the use of the GAL4 system to drive GFP expression during metamorphosis should provide a valuable new tool for defining the molecular mechanisms that regulate this critical transition in the insect life cycle.

Online supplementary data. The movies listed here are derived from data described in each figure. See the corresponding figure number for details. All movies can be accessed through the ScienceDirect website at http://www.sciencedirect.com, or the Thummel lab website at http://thummel.genetics.utah.edu. Movie 1A: Translocation and destruction of the larval salivary glands in an early pupa, visualized from the ventral side. Movie 1B: Translocation and destruction of the larval salivary glands in the early pupa, visualized from the lateral side. Movie 2: Destruction of the larval abdominal muscles. Movie 3: Salivary glands fail to die in *rbp*[5] mutants. Movie 4: Muscles fail to die in *rbp*[5] mutants. Movie 5: Imaginal disc morphogenesis and head eversion establish the basic body plan of the adult fly. Movie 6: Movement of a T1 leg in an early prepupa and pupal morphogenetic events. Movie 7: *br*[5] mutants display no eversion or elongation of leg imaginal discs. Movie 8: *crol*[3] mutants display defects in adult leg morphogenesis.

References

Bate, M., 1993. The mesoderm and its derivatives, in: Bate, M., Martinez Arias, A. (Eds.), The Development of *Drosophila melanogaster*, Vol. II, Cold Spring Harbor Laboratory Press, Cold Spring Harbor, NY, pp. 1013–1090.

Belyaeva, E.S., Aizenzon, M.G., Kiss, I.I., Gorelova, T.D., Pak, S., Umbetova, G., Kramers, P., Zhimulev, I.F., 1982. New mutants. Drosophila Inform. Serv. 58, 184–190.

Belyaeva, E.S., Aizenzon, M.G., Semeshin, V.F., Kiss, I.I., Koczka, K., Baritcheva, E.M., Gorelova, T.D., Zhimulev, I.F., 1980. Cytogenetic analysis of the 2B3-4-2B11 region of the X-chromosome of *Drosophila melanogaster*. I. Cytology of the region and mutant complementation groups. Chromosoma 81, 281–306.

Bodenstein, D., 1965. The postembryonic development of *Drosophila*, in: Demerec, M. (Ed.), Biology of *Drosophila*, Hafner Publishing Co., New York, pp. 275–367.

Chadfield, C.G., Sparrow, J.C., 1985. Pupation in *Drosophila melanogaster* and the effect of the *lethalcryptocephal* mutation. Dev. Genet. 5, 103–114.

Cohen, S., 1993. Imaginal disc development, in: Bate, M., Martinez Arias, A. (Eds.), The Development of *Drosophila melanogaster*, Vol. II, Cold Spring Harbor Laboratory Press, Cold Spring Harbor, NY, pp. 747–841.

Condic, M.L., Fristrom, D., Fristrom, J.W., 1991. Apical cell shape changes during *Drosophila* imaginal leg disc elongation: a novel morphogenetic mechanism. Development 111, 23–33.

Crossley, A.C., 1978. The morphology and development of the *Drosophila* muscular system, in: Ashburner, M., Wright, T.R.F. (Eds.), The Genetics and Biology of *Drosophila*, Vol. 2b, Academic Press, New York, pp. 499–560.

D'Avino, P.P., Thummel, C.S., 1998. crooked legs encodes a family of zinc finger proteins required for leg morphogenesis and ecdysone-regulated gene expression during *Drosophila* metamorphosis. Development 125, 1733–1745.

D'Avino, P.P., Thummel, C.S., 2000. The ecdysone regulatory pathway controls wing morphogenesis and integrin expression during *Drosophila* metamorphosis. Dev. Biol. 220, 211–224.

DiBello, P.R., Withers, D.A., Bayer, C.A., Fristrom, J.W., Guild, G.M., 1991. The *Drosophila Broad-Complex* encodes a family of related proteins containing zinc fingers. Genetics 129, 385–397.

Fristrom, D., Fristrom, J.W., 1993. The metamorphic development of the adult epidermis, in: Bate, M., Martinez Arias, A. (Eds.), The Development of *Drosophila melanogaster*, Vol. II, Cold Spring Harbor Laboratory Press, Cold Spring Harbor, NY, pp. 843–897.

Gilbert, L., Tata, J., Atkinson, B., 1996. Metamorphosis: Postembryonic Reprogramming of Gene Expression in Amphibian and Insect Cells. Academic Press, New York.

Jiang, C., Baehrecke, E.H., Thummel, C.S., 1997. Steroid regulated programmed cell death during *Drosophila* metamorphosis. Development 124, 4673–4683.

Jiang, C., Lamblin, A.-F.J., Steller, H., Thummel, C.S., 2000. A steroid triggered transcriptional hierarchy controls salivary gland cell death during *Drosophila* metamorphosis. Mol. Cell 5, 445–455.

Karim, F.D., Guild, G.M., Thummel, C.S., 1993. The *Drosophila Broad-Complex* plays a key role in controlling ecdysone-regulated gene expression at the onset of metamorphosis. Development 118, 977–988.

Kiss, I., Beaton, A.H., Tardiff, J., Fristrom, D., Fristrom, J.W., 1988. Interactions and developmental effects of mutations in the *Broad-Complex* of *Drosophila melanogaster*. Genetics 118, 247–259.

Lee, C.Y., Baehrecke, E.H., 2001. Steroid regulation of autophagic programmed cell death during development. Development 128, 1443–1455.

Menon, S.D., Chia, W., 2001. *Drosophila* rolling pebbles: a multido-
    main protein required for myoblast fusion that recruits D-Titin in
    response to the myoblast attractant Dumbfounded. Dev. Cell 1,
    691–703.
Milner, M., Bleasby, A., Kelly, S., 1984. The role of the peripodial
    membrane of leg and wing imaginal discs of *Drosophila melanogaster*
    during evagination and differentiation in vitro. Roux's Arch. Dev. Biol.
    193, 180–186.
Restifo, L.L., White, K., 1992. Mutations in a steroid hormone-regulated
    gene disrupt the metamorphosis of internal tissues in *Drosophila*:
    salivary glands, muscle, and gut. Roux's Arch. Develop. Biol. 201,
    221–234.
Richards, G., 1981. Insect hormones in development. Biol. Rev. 56, 501–
    549.
Richards, G., 1997. The ecdysone regulatory cascades in Drosophila. Adv.
    in Dev. Biol. 5, 81–135.
Riddiford, L.M., 1993. Hormones and *Drosophila* development, in: Bate,
    M., Martinez-Arias, A. (Eds.), The Development of *Drosophila mela-
    nogaster*, Vol. II, Cold Spring Harbor Laboratory Press, Cold Spring
    Harbor, NY, pp. 899–939.

Robertson, C.W., 1936. The metamorphosis of *Drosophila melanogaster,*
    including an accurately timed account of the principal morphological
    changes. J. Morphol. 59, 351–399.
Russell, S., Ashburner, M., 1996. Ecdysone-regulated chromosome puffing in
    Drosophila melanogaster, in: Atkinson, B.G., Gilbert, L.I., Tata, J.R.
    (Eds.), Metamorphosis. Postembryonic Reprogramming of Gene Expression
    in Amphibian and Insect Cells, Academic Press, New York, pp. 109–144.
Thummel, C.S., 1996. Flies on steroids—*Drosophila* metamorphosis and
    the mechanisms of steroid hormone action. Trends Genet. 12, 306–310.
Usui, K., Simpson, P., 2000. Cellular basis of the dynamic behavior of the
    imaginal thoracic discs during *Drosophila* metamorphosis. Dev. Biol.
    225, 13–25.
von Kalm, L., Fristrom, D., Fristrom, J., 1995. The making of a fly leg: a
    model for epithelial morphogenesis. Bioessays 17, 693–702.
Wahl, B., 1914. Über die Kopfbildung cyclorapher Dipteran larven und die
    postembryonale entwicklung des fliegenkopfes. Arb. Zool. Inst. Univ.
    Wien 20, 159–272.
Zhimulev, I.F., Belyaeva, E.S., Mazina, O.M., Balasov, M.L., 1995. Struc-
    ture and expression of the *BR-C* locus in *Drosophila melanogaster*
    (Diptera: Drosophilidae). Eur. J. Entomol. 92, 263–270.